BIOCHEMISTRY
including biophysical chemistry & molecular biology

Article

pubs.acs.org/biochemistry

Thermodynamic and Kinetic Analysis of Peptides Derived from CapZ, NDR, p53, HDM2, and HDM4 Binding to Human S100B

Lucas N. Wafer, Werner W. Streicher,† Scott A. McCallum, and George I. Makhatadze*

Center for Biotechnology and Interdisciplinary Studies and Department of Biology, Rensselaer Polytechnic Institute, 110 8th Street, Troy, New York 12180, United States

Supporting Information

ABSTRACT: S100B is a member of the S100 subfamily of EF-hand proteins that has been implicated in malignant melanoma and neurodegenerative conditions such as Alzheimer's disease and Parkinson's disease. Calcium-induced conformational changes expose a hydrophobic binding cleft, facilitating interactions with a wide variety of nuclear, cytoplasmic, and extracellular target proteins. Previously, peptides derived from CapZ, p53, NDR, HDM2, and HDM4 have been shown to interact with S100B in a calcium-dependent manner. However, the thermodynamic and kinetic basis of these interactions remains largely unknown. To gain further insight, we screened these peptides against the S100B protein using isothermal titration calorimetry and nuclear magnetic resonance. All peptides were found to have binding affinities in the low micromolar to nanomolar range. Binding-induced changes in the line shapes of S100B backbone ^{1}H and ^{15}N resonances were monitored to obtain the dissociation constants and the kinetic binding parameters. The large microscopic K_{on} rate constants observed in this study ($\geq 1 \times 10^{7}$ M^{-1} s^{-1}) suggest that S100B utilizes a "fly casting mechanism" in the recognition of these peptide targets.

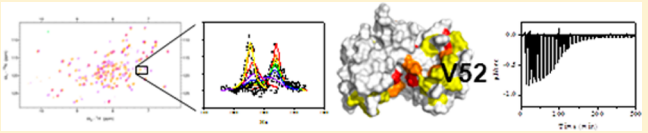

The S100 protein family consists of small (9−13 kDa), dimeric, calcium-binding proteins that are unique to vertebrates.[1] These proteins play a role in a variety of cell functions, including phosphorylation,[2,3] enzyme regulation,[4,5] and cytoskeleton dynamics,[6] and have also been implicated in a variety of cancers,[7−10] inflammatory conditions,[11−13] and neurological diseases.[14−17] Unlike calmodulin, a ubiquitous calcium-binding protein, expression patterns of S100 protein family members appear to be cell specific, with individual expression levels depending on local environmental factors.[18] Each monomer consists of four α-helices and contains two calcium-binding domains: a high-affinity, canonical EF-hand in the C-terminus and a low-affinity "pseudo" EF-hand in the N-terminus.[19] The disparity in calcium binding affinity between the two sites is much greater than that seen in the different isoforms of parvalbumins and originates in local sequence differences rather than long-range contacts.[20−22] Cation binding induces a large conformational change, during which helix 3 reorients itself ∼90° relative to helix 4.[23−29] This exposes a large patch of hydrophobic surface area that is generally required for protein binding and various S100 functions.[30]

S100B is the best studied member of the S100 family and was the first to be discovered.[31] To date, more than 29 structures of the protein have been deposited in the Protein Data Bank (PDB).[32] These include both crystallographic and solution NMR studies that span all functionally relevant states (apo, cation-bound, and peptide-bound) and orthologs from three species (*Homo sapiens*, *Rattus norveggicus*, and *Bos taurus*). S100B is known to interact with more than 20 targets, including nuclear, cytoplasmic, and extracellular ligands.[30] It has established roles in Parkinson's, Alzheimer's, and Down syndrome, and it is currently the best prognostic marker for malignant melanoma.[15−17,33] Previously, it has been shown to interact with peptides derived from CapZ,[34,35] p53,[36−38] NDR,[5] MDM2/HDM2,[39,40] and MDM4/HDM4.[39] Despite the large amount of data concerning the identification of the binding targets, ambiguity about the structural, thermodynamic, and kinetic basis of these interactions remains.

The TRTK12 peptide is derived from the C-terminal region of the actin-capping protein CapZ (residues 265−276) but was originally identified as a S100B binding motif using a random phage display library. The consensus sequence (K/R)(L/I)XWXXIL was shown to compete with known S100B binding partners, including CapZ and glial fibrillary acidic protein, in a calcium-dependent manner.[34] Previous studies had identified helix 3, the hinge region, and helix 4 as the most likely regions for target recognition, because of their structural rearrangement during calcium binding and their sequence divergence among the S100 proteins.[5,36,38,39,41−45] Mapping of the interaction surface by NMR identified residues involved in binding the TRTK12$^{(265-276)}$ peptide and provided an important step in confirming the target binding site for S100B. TRTK12$^{(265-276)}$ also helped establish the tendency for binding-competent peptides to have Arg or Lys residue(s) in addition to hydrophobic residues.[46]

Received: June 27, 2012
Revised: August 21, 2012
Published: August 22, 2012

The p53 protein is a transcription activator that upregulates genes critical to cell cycle arrest and apoptosis.[47] If this protein is mutated or downregulated, cell proliferation can proceed unchecked, and otherwise healthy cells proliferate and become cancerous. Conversely, if this protein is upregulated, premature aging and cell damage can occur.[48] The p53 protein consists of an N-terminal transactivation domain, a DNA-binding domain, a tertamerization domain, and a C-terminal regulation domain. S100B has been shown to bind to individual subdomains with varying affinities in a complex manner, depending on the oligomerization state of p53 and its post-translational modifications.[37,49,50] S100B preferentially binds to the tetramerization domain of p53 during basal expression, preventing the more active tetrameric form of p53 from entering the nucleus. Binding to the extreme C-terminus prevents protein kinase C-dependent phosphorylation of Ser376 and Ser378.[49] Interestingly, this region is unstructured both as a functional domain in the p53 protein and as a free peptide in solution.[51−53] Upon binding S100B, this sequence adopts a partially helical structure.[29,54−56]

Nuclear Dbf2-related kinases (NDR's) make up a subgroup of the serine/threonine AGC kinases and are highly conserved among eukaryotes.[57] NDR activity is critical to mitotic progression, cytokinesis, morphological changes, cell proliferation, and apoptosis.[57] S100B binds to a basic/hydrophobic sequence at the junction of the N-terminal regulatory and catalytic domains.[5] Mutagenesis studies have shown that Thr74 plays a crucial role in binding, and it is likely that S100B binding triggers autophosphorylation of Ser281, activating the kinase.[58] Like the p53 protein, the S100B binding site of NDR includes an unstructured region that adopts a three-turn helical structure upon complex formation.[5]

Human double minute 2 (HDM2) and human double minute 4 (HDM4) proteins are both critical regulators of p53.[59] The former acts as a tumor suppressor by binding to p53 and inhibiting N-terminal activation, as well as targeting the protein for ubiquitin-dependent proteosomal degradation.[60] The latter acts in a more complex fashion, either inhibiting p53's apoptotic activity or stabilizing the protein and promoting the mitochondrial apoptotic response.[61] In addition, HDM4 has been shown to form heterodimers with HDM2, which adds an additional layer of regulation to the activity and effective concentration of the HDM2 protein.[62] S100B has been shown to interact with peptides derived from the N-terminal domains of both proteins, as well as the full-length HDM2 protein.[39,40] It is still unclear whether interactions with these binding sites are physiologically relevant. The HDM2$^{(25-47)}$ peptide, consisting of residues 25−47 of the full-length protein, is derived from a region that is buried in the three-dimensional structure.[39] In contrast, the HDM4 protein appears to be intrinsically more flexible, adopting several conformations in the unbound state.[63] The HDM2$^{(25-47)}$ and HDM4$^{(25-47)}$ peptides, both consisting of residues 25−47, were identified on the basis of the similarity of their sequence to that of TRTK12.[39] Competition experiments using a phage display have demonstrated that the binding site for the full-length HDM2$^{(25-47)}$ protein at least partially overlaps with the binding site for TRTK12$^{(265-276)}$.[5,39,40] In addition, no structure of S100B bound to either target exists. Interestingly, the available data suggest these peptides may interact with S100B through a unique and asymmetric mechanism.[40]

Here, we performed a full thermodynamic and kinetic characterization of the TRTK12$^{(265-276)}$, p53$^{(367-388)}$, NDR$^{(62-87)}$, HDM2$^{(25-47)}$, and HDM4$^{(25-47)}$ peptides binding to the S100B protein. All peptides were found to have dissociation constants in the low micromolar to nanomolar range, as determined by isothermal titration calorimetry (ITC) and nuclear magnetic resonance (NMR). In addition, experimentally measured changes in the heat capacity upon binding were found to be in excellent agreement with predicted values in structure-based calculations that take into account changes in solvation upon binding. Binding-induced changes in the chemical shift of S100B backbone ^{1}H and ^{15}N resonances were monitored to confirm the binding site for these peptides and to obtain the kinetic parameters of binding. The relatively fast microscopic on rate constants observed in this study suggest that S100B utilizes a "fly casting mechanism" or "folding after binding" in the recognition of these peptide targets.

EXPERIMENTAL PROCEDURES

Protein and Peptide Purification. Unlabeled and doubly labeled [^{15}N,^{13}C]human S100B proteins were overexpressed in *Escherichia coli* and purified as previously described.[64−66] The protein concentration was determined using a molar extinction coefficient at 280 nm (ε_{280}) of 1490 M^{-1} cm^{-1}. All peptides, with their N-termini acetylated and their C-termini amidated, were synthesized using standard Fmoc chemistry at the Penn State College of Medicine Macromolecular Core Facility. The TRTK12$^{(265-276)}$ peptide derived from the actin-binding protein CapZ (Ac-TRTKIDWNKILS-Am), the nuclear Dbf2-related kinase [NDR$^{(62-87)}$; amino acid sequence, Ac-KRLRRSAHARKETEFLRLKRTRLGLEY-Am], and the C-terminal p53 peptide [p53$^{(367-388)}$; amino acid sequence, Ac-YSHLKSKKGQSTSRHKKLMFKTE-Am] have all previously been used in structural studies.[5,35,36,67] The human homologue of marine double minute 2 peptide [HDM2$^{(25-47)}$; amino acid sequence, Ac-ETLVRPKPLLLKLLKSVGAY-Am] and the human homologue of marine double minute 4 peptide [HDM4$^{(25-47)}$; amino acid sequence, Ac-NQVRPKLPLLKIL-HAAGAQY-Am] are the same sequences used by Weber et al.[36,39] With the exception of TRTK12$^{(265-276)}$, all peptides have an additional Tyr residue on their N-termini or C-termini, to allow for quantification by UV absorbance spectroscopy. For the NDR$^{(62-87)}$ and p53$^{(367-388)}$ peptides, this residue is known to exist outside of the binding site in an unstructured region of the peptide and is expected to have little to no impact on binding.[5,29] Similarly, the sequence alignment data for the HDM2$^{(25-47)}$ and HDM4$^{(25-47)}$ peptides suggest that the extreme C-termini exist outside of the S100B binding motif.[39] The peptides were purified as previously described,[65] and their masses were confirmed via mass spectrometry. The concentration of peptides was determined using molar extinction coefficients at 280 nm (ε_{280}) of 5500 M^{-1} cm^{-1} for TRTK12$^{(265-276)}$ and 1490 M^{-1} cm^{-1} for p53$^{(367-388)}$, NDR$^{(62-87)}$, HDM2$^{(25-47)}$, and HDM4$^{(25-47)}$.[68]

Isothermal Titration Calorimetry (ITC). ITC measurements were performed using a VP-ITC instrument (MicroCal, Inc., Northhampton, MA) as previously described.[65,69,70] Prior to all experiments, the protein and peptide were dialyzed with two buffer changes of 20 mM Tris base, 0.2 mM disodium EDTA, 1 mM TCEP (pH 7.5), and 5 mM calcium chloride at room temperature. For the p53$^{(367-388)}$ peptide, the "high-salt" buffer included an additional 120 mM NaCl. In general, 0.4−1.6 mM peptide was injected in 2−7 μL increments into the sample cell (1.5 mL) containing 20−50 μM protein. For the

titration of Ca^{2+}-S100B and HDM4$^{(25-47)}$, the protein solution was injected into the cell containing the peptide solution. Experiments were performed in the temperature range from 5 to 35 °C, in 5 °C increments, except in cases where the heat effects were close to zero and thus there was insufficient signal. The heat of dilution was measured prior to each experiment by performing four peptide injections into buffer, using the experimental concentrations and volumes. It was found to be negligible for all peptides over the temperature and volume ranges reported. The resulting titration curves were analyzed using the Origin for ITC software supplied by MicroCal (Northampton, MA).

It is important to note that ITC data analysis is model-dependent. In the absence of additional information, analysis is performed by examining models in order of increasing complexity. In accordance with Occam's razor, the simplest model that fits all the available data is assumed to be correct. The following binding models were considered.

Single-binding site model, with one peptide per S100B dimer:[71]

$$Q = \frac{n[\text{cell}]_t \Delta H_{cal} V_o}{2}\left(A - \sqrt{A^2 - \frac{4[\text{syringe}]_t}{n[\text{cell}]_t}}\right) \quad (1)$$

where Q is the integral heat at each injection, $A = 1 + [\text{syringe}]_t/(n[\text{cell}]_t) + [\text{syringe}]_t/[n(1/K_d)[\text{cell}]_t]$, $n = 1$ is the stoichiometry of the protein−peptide complex, $[\text{syringe}]_t$ is the total concentration of the peptide/protein solution in the ITC syringe, $[\text{cell}]_t$ is the total concentration of the protein/peptide solution in the ITC cell, and K_a is the association constant.

Two-identical binding sites model, with two peptides per S100B dimer:[71]

$$Q = \frac{n[\text{cell}]_t \Delta H_{cal} V_o}{2}\left(A - \sqrt{A^2 - \frac{4[\text{syringe}]_t}{n[\text{cell}]_t}}\right) \quad (2)$$

where Q is the integral heat at each injection, $A = 1 + [\text{syringe}]_t/(n[\text{cell}]_t) + [\text{syringe}]_t/[n(1/K_d)[\text{cell}]_t]$, and $n = 2$ is the stoichiometry of the protein−peptide complex.

Two-sequential binding sites model, with two peptides per S100B dimer:[71]

$$\begin{aligned} Q = {} & [\text{cell}]_t V_o\{[\Delta H_{cal1}(1/K_{d1})[\text{syringe}]_t \\ & + (\Delta H_{cal1} + \Delta H_{cal2})(1/K_{d1})(1/K_{d2})[\text{syringe}]_t{}^2] \\ & /[1 + [\text{syringe}]_t(1/K_{d1}) + 1 + (1/K_{d1})(1/K_{d2}) \\ & [\text{syringe}]_t{}^2]\} \end{aligned} \quad (3)$$

where Q is the integral heat at each injection, K_1 and K_2 are the association constants for binding to sites 1 and 2, respectively, and ΔH_{cal1} and ΔH_{cal2} are the calorimetric enthalpies for binding to sites 1 and 2, respectively.

Far-UV Circular Dichroism. The far-UV CD spectra (260−195 nm) of the TRTK12$^{(265-276)}$, p53$^{(367-388)}$, NDR$^{(62-87)}$, HDM2$^{(25-47)}$, and HDM4$^{(25-47)}$ peptides were measured on a Jasco-715 spectropolarimeter in a 1 mm light path-length cuvette. Measurements were performed using 50 μM peptide in the presence of 20 mM Tris, 1 mM TCEP, and 0.2 mM EDTA (pH 7.5) with or without 5 mM calcium and with or without 30% TFE. Ellipticity values (Θ) for the peptides were corrected by subtracting the corresponding values for the buffer and converting them to mean residue ellipticity, [Θ], using the following equation:

$$[\Theta] = \Theta \times \text{MR}/(10lc) \quad (4)$$

where MR is the mean molecular mass of the amino acids in each peptide, l is the optical path length in centimeters, and c is the peptide concentration in milligrams per milliliter. The fraction helicity, f_H, was calculated as

$$f_H = \frac{[\Theta]_{222} - [\Theta]_C}{[\Theta]_H - [\Theta]_C} \quad (5)$$

where $[\Theta]_{222}$ is the experimentally determined ellipticity at 222 nm, $[\Theta]_C$ is the ellipticity of the fully coiled state, and $[\Theta]_C$ is the ellipticity of the fully helical state.

The ellipticity of the fully coiled state, $[\Theta]_C$, has a temperature dependence described as[72]

$$[\Theta]_C = 640 - 45T \quad (6)$$

where T is the temperature in degrees Celsius. The ellipticity of the fully helical state, $[\Theta]_H$, for a protein or peptide consisting of N_r residues, has a temperature dependence described by[72]

$$[\Theta]_H = (-40000 + 250T)\left(1 - \frac{2.5}{N_r}\right) \quad (7)$$

where N_r is the number of residues.

Structure-Based Calculation of ΔC_p. Structure-based calculations allow for cross validation of thermodynamic parameters obtained from protein−ligand binding.[65,73] Most often, these calculations of the heat change upon binding, ΔC_p, are based on changes in the accessible surface area upon binding, ΔASA_{tot}, of the ligand to the protein. Using the available three-dimensional structures of S100B in complex with the studied peptides, ΔASA_{tot} was modeled as previously described.[74] In cases where no structure was available, homology models of the peptide-bound state were generated using Modeler[75] and PDB entry 1DT7.[29] Changes in the accessible surface area upon binding were calculated as follows:

$$\Delta\text{ASA}_{tot} = \text{ASA}_{dim+pep} - (\text{ASA}_{dim-pep} + \text{ASA}_{unf\,pep}) \quad (8)$$

where ΔASA_{tot} is the total change in the accessible surface area upon peptide binding, $\text{ASA}_{dim+pep}$ is the ASA of the protein in complex with the peptide, $\text{ASA}_{dim-pep}$ is the ASA of the protein in the absence of peptide, and $\text{ASA}_{unf\,pep}$ is the ASA of the unfolded peptide. As described previously,[65,73,76] changes in ΔASA were subdivided into four categories (aliphatic surface area, aromatic surface area, peptide backbone surface area, and polar surface area) and converted into ΔC_p using the following empirical relationship:

$$\begin{aligned} \Delta C_p = {} & 2.14 \times \Delta\text{ASA}_{alp} + 1.55 \times \Delta\text{ASA}_{arm} \\ & - 1.81 \times \Delta\text{ASA}_{bb} - 0.88 \times \Delta\text{ASA}_{pol} \end{aligned} \quad (9)$$

where ΔASA_{alp} values are the changes in ASA for aliphatic amino acids, ΔASA_{arm} values are the changes in ASA for aromatic amino acids, ΔASA_{pol} values are the changes in ASA for polar amino acids, and ΔASA_{bb} values are the changes in ASA for the polypeptide backbone.

NMR Spectroscopy. NMR spectra were collected at 35 °C on a Bruker AVANCE II 600 MHz spectrometer equipped with a triple-resonance cryoprobe with z-axis gradients and processed using the Bruker software suite TopSpin (version 2.1). Backbone resonance assignments were obtained for S100B in the peptide-free state using the auto assignment

dx.doi.org/10.1021/bi300865g | Biochemistry 2012, 51, 7189−7201

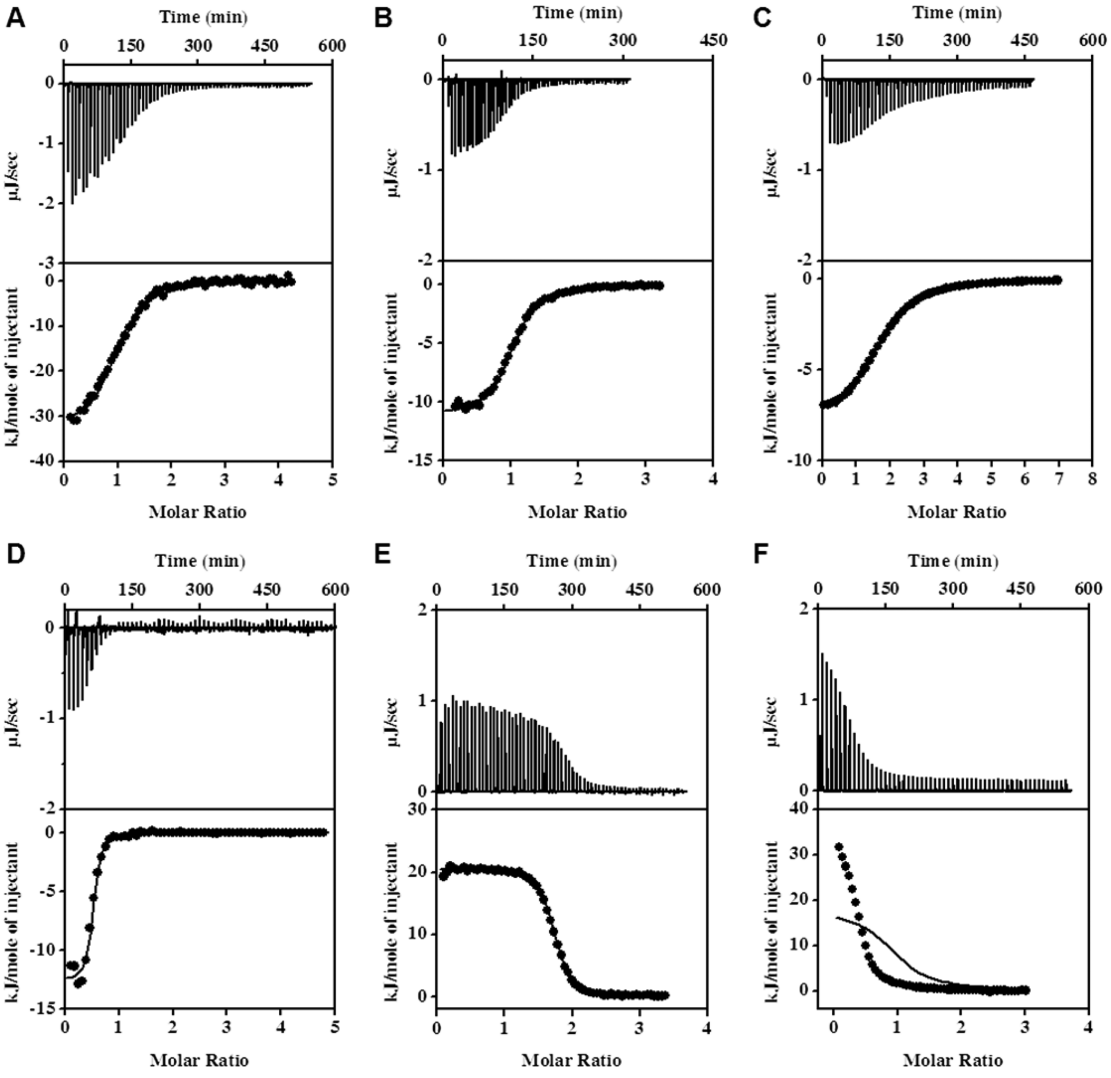

Figure 1. Examples of ITC experiments showing the binding of p53, TRTK12, NDR, HDM2, and HDM4 peptides to S100B in the presence of calcium. Plots represent the raw heat effects (microjoules per second) as a function of time, the cumulative heat effects (kilojoules per mole, represented by ●) as a function of the molar ratio of peptide to protein, and the fits to the experimental data (—) for binding of p53 to S100B at 25 °C (A, data fit to eq 2), binding of TRTK12 to S100B at 25 °C (B, data fit to eq 2), binding of NDR to S100B at 30 °C (C, data fit to eq 3), binding of HDM2 to S100B at 35 °C (D, data fit to eq 2), binding of HDM4 to S100B at 10 °C (E, data fit to eq 2), and binding of HDM2 to S100B at 15 °C (F, data fit to eq 1).

program MONTE with the connectivities detected in the spectra of the HNCO, HN(CA)CO, HNCACB, and HN(CO)CACB triple-resonance experiments as input and validated against previously published assignments.[77] Reassignments of the amide groups in the peptide-bound state were determined by monitoring changes in chemical shifts in a series of two-dimensional (2D) $^{1}H-^{15}N$ HSQC spectra acquired throughout the peptide titrations and were verified against published assignments when applicable.[5,24,27,29,78] Prior to all experiments, the protein and peptide were simultaneously dialyzed into buffer containing 5 mM Tris, 15 mM NaCl, and 0.34 mM NaN_3 (pH 7.5). After dialysis, 5% D_2O and 10 mM $CaCl_2$ were added to the samples. Chemical shift mapping experiments were performed by titrating 0−4 mM peptide into 0.1−0.45 mM calcium-bound S100B and monitoring changes in backbone ^{15}N and ^{1}H. All titrations were continued until there were no longer observable changes in either the ^{15}N or ^{1}H chemical shifts. The combined changes in the proton and nitrogen chemical shifts were quantified according to the following weighted distance metric:[79,80]

$$\sqrt{\delta_N{}^2 + (5\delta_H)^2} \quad (10)$$

where δ_N and δ_H are the changes in chemical shift (parts per million) in the nitrogen and proton dimensions, respectively. Spectra were analyzed using Sparky.[81]

LineShapeKin Analysis. Line shape analysis was performed using the BiophysicsLab Matlab package.[82] The one-dimensional slices of the ^{15}N and ^{1}H dimensions from 2D HSQCs were extracted in Sparky,[81] and the intensities were normalized by the area under each peak to account for exchange broadening in the other dimension.[82] For the TRTK12$^{(265-276)}$ and p53$^{(367-388)}$ peptides, titration data were fit to a model in which there are two identical binding sites per S100B dimer, or one peptide interacting with each S100B monomer. The sequential binding model cannot be explicitly modeled using LineShapeKin, so the titration data for the NDR$^{(62-87)}$ peptide were fit to a model in which there are two

dx.doi.org/10.1021/bi300865g | *Biochemistry* 2012, 51, 7189−7201

identical binding sites per S100B dimer and compared to the simulated data using a sequential binding model[83] to estimate the upper and lower limits on the kinetic rate constants. For the HDM2$^{(25-47)}$ and HDM4$^{(25-47)}$ peptides, binding was best fit to a single binding site per S100B dimer. The software analytically solves for both the apparent binding constant, K_d^{App}, and the off rate, K_{off}, simultaneously, which allows the on rate, K_{on}, to be readily calculated. The x^2 values were examined in a 2D matrix as a function of binding affinity and K_{off} rates to ensure the data were fitting to a true global minimum (see the Supporting Information). For data to qualify for line shape analysis, the amide peak must have been determined to have undergone a significant chemical shift change, not overlap with any other amide peak, and be sufficiently resolved in all spectra of the titration series. For each peptide, 6−10 residues were found to meet these criteria. As part of the analysis, all residue specific data were assumed to be reporting on the same binding event. As a result, fitted parameters, including the rate constants for binding kinetics, could be calculated with greater certainty in global fits using all data. To validate this assumption, individual residues were independently fit and these results were compared to each other, as well as the global analysis, and found to be in good agreement (see the Supporting Information). All reported values are the result of global fits, which include both ^{15}N and ^{1}H dimensions of all relevant amide groups across all ligand concentrations.

RESULTS

Thermodynamics of Peptide Binding. ITC is a powerful, quantitative method for measuring the thermodynamics of protein−ligand interactions. It is unique in its ability to simultaneously determine the enthalpy (ΔH_{cal}), affinity (K_d), and stoichiometry (n) of an interaction from a single experiment at a given temperature.[70,84] In addition, if experiments are performed over a range of temperatures, one can derive the heat capacity change upon binding (ΔC_p) from the temperature dependence of the enthalpy of binding. An important caveat is that all data analysis is model-dependent and the simplest model that accurately fits the data is assumed to be correct.

Below we present the results of analysis of five different peptides binding to calcium-saturated S100B, i.e., Ca^{2+}-S100B. For readability, it will henceforth be termed simply S100B.

TRTK12. Figure 1A shows representative ITC data from experiments in which the TRTK12$^{(265-276)}$ peptide was titrated into S100B. The titration data are best fit to the simplest model, where there are two identical binding sites per S100B dimer (eq 2). This stoichiometry is consistent with previous structural studies that show each S100B monomer has an identical binding site.[29,37,46,54,85] The binding affinity per site is determined to be 2 ± 1 μM at 25 °C, which is in good agreement with fluorescence and the weaker values from the conflicting reports from NMR-based assays.[54,86] Figure 2 shows the dependence of the enthalpy of binding, ΔH_{cal}, on temperature. This dependence is a linear function of temperature, and the slope of the dependence is the heat capacity change upon binding, ΔC_p. It has previously been shown for a variety of protein−protein and protein−peptide interactions that ΔC_p can be accurately predicted using structure-based calculations.[73,74] The heat capacity change for the S100B−TRTK12$^{(265-276)}$ interaction is not an exception, as the experimentally obtained ΔC_p (−1.3 ± 0.2 kJ mol^{-1} K^{-1}) is in excellent agreement with the calculated value based on the bound complex (PDB entry 1MQ1) (−1.2 ± 0.1 kJ mol^{-1} K^{-1}) (eq 9).

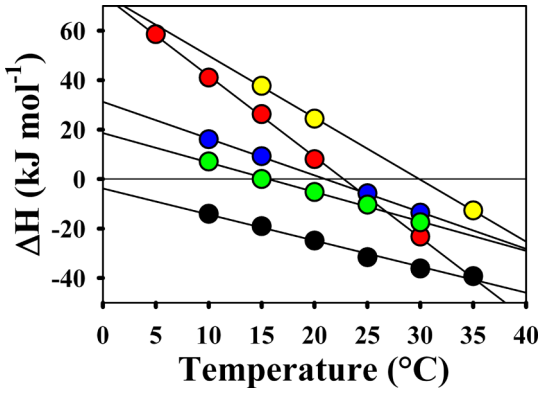

Figure 2. Temperature dependence of the enthalpies, ΔH_{cal}, of the TRTK12 (green circles), p53 (black circles), NDR (blue circles), HDM2 (yellow circles), and HDM4 (red circles) peptides binding to the S100B protein in the presence of 5 mM calcium. Solid lines represent linear fits of the ΔH_{cal} temperature dependencies for each S100−peptide interaction. The slopes of these lines represent the experimental changes in heat capacity, which are summarized in Table 1.

p53. Figure 1B shows the typical ITC titration profile for the p53$^{(376-388)}$ peptide binding to the S100B protein. The titration data fit well to the simplest model, where there are two identical and independent binding sites per S100B dimer. The dissociation constant, K_d, for each site in the presence of a low salt concentration was determined to be 2 ± 1 μM, which is in agreement with kinetic phosphorylation assays.[3] The dissociation constant in the presence of a high salt concentration is an order of magnitude weaker (20 ± 5 μM). An increasing ioninc strength has been shown to significantly reduce the affinity of the p53 peptide for S100B,[39,49] although the absolute affinity reported here is somewhat tighter than previously reported values measured using competitive binding assays[39] and ultracentrifugation experiments. Figure 2 shows the linear dependence of the enthalpy of binding, ΔH_{cal}, on temperature for the low-salt conditions, although it should be noted that the experimentally determined ΔC_p values did not change significantly in the presence or absence of salt (−1.2 ± 0.1 or −1.0 ± 0.1 kJ mol^{-1} K^{-1}, respectively). The calculated ΔC_p (−1.0 ± 0.1 kJ mol^{-1} K^{-1}) (PDB entry 1DT7) is well within error of these values (Table 1).

NDR. Figure 1C shows results from representative ITC experiments in which the NDR$^{(62-88)}$ peptide was titrated into Ca^{2+}-S100B. The titration data could not be accurately fit to the simplest binding model, where there are two identical binding sites per S100B dimer (eq 2). The data appear to fit well to the more complex sequential binding site model, where there are two nonidentical, interacting sites per S100B dimer (eq 3). This model is consistent with the previously reported stoichiometry,[5] i.e., two peptides per S100B dimer. However, it delineates a significantly different mechanism of binding for the NDR peptide as compared to the TRTK12 or p53 peptides. This model suggests that binding of the first NDR peptide transduces a structural change across the S100B dimer that changes the affinity for the second NDR peptide. The higher-affinity site has a K_{d1} of 0.4 ± 0.2 μM, while the lower-affinity site has a K_{d2} of 2 ± 1 μM. The sequential binding model has been observed before for other S100 proteins interacting with target peptides. The negative cooperativity (K_{d1} < K_{d2})

dx.doi.org/10.1021/bi300865g | *Biochemistry* 2012, 51, 7189−7201

Table 1. Summary of the Thermodynamic Properties of Binding of S100B to p53, TRTK12, NDR, HDM2, and HDM4 Determined Using ITC Experiments and Comparison with Structure-Based Calculations

peptide	K_d (μM)	$\Delta C_{p,exp}$ (kJ mol^{-1} K^{-1})	$\Delta C_{p,calc}$ (kJ mol^{-1} K^{-1})
TRTK12	2 ± 1	−1.3 ± 0.2	−1.1 ± 0.1
p53, low salt	2 ± 1	−1.0 ± 0.1	−1.0 ± 0.1
p53, high salt	20 ± 5	−1.2 ± 0.3	−1.0 ± 0.1
NDR	2 ± 1, 0.4 ± 0.2[a]	−1.5 ± 0.3	−1.9 ± 0.2
HDM2	0.5 ± 0.2	−1.3 ± 0.2	−1.0 ± 0.1[b]
HDM4	0.07 ± 0.03	−1.7 ± 0.2	−0.7 ± 0.1[b]

[a]The interaction between S100B and NDR was fit to a sequential binding model, where each S100B monomer had a unique binding affinity. [b]These values were calculated using homology models of the S100B dimer (PDB entry 1DT7) binding to two peptides.

observed here is similar to that observed for the MDM2 N-terminal domain binding to S100B,[40] but in contrast to the positive cooperativity ($K_{d1} > K_{d2}$) observed for the binding of Annexin II to S100A10.[65] Consistent with the sequential binding model, the enthalpies of binding for each site are also different. The temperature dependence of the sum of the individual enthalpies of binding is listed in Table 1. The change in heat capacity for the S100B−NDR interaction is shown in Figure 2. It is important to note that the structure-based calculation for ΔC_p can only be conducted for the final bound complex (two peptides per S100B dimer) and not any intermediate states. It is this value that is then compared with the temperature dependence of the total enthalpy of binding, or the sum of the individual enthalpies of binding. In this case, the calculated and experimentally determined ΔC_p values agree within error [−1.5 ± 0.3 kJ mol^{-}K^{-1} (PDB entry 1PSB) and −1.9 ± 0.2 kJ mol^{-}K^{-1}, respectively], providing internal consistency for the data analysis.

HDM2 and HDM4. Panels D and E of Figure 1 show typical ITC profiles for the HDM2 and HDM4 peptides binding to S100B. The simplest model, in which there are two identical binding sites per S100B dimer, was insufficient to fit the binding isotherms (Figure 1E). Subsequently, binding data for the HDM2$^{(25-47)}$ and HDM4$^{(25-47)}$ peptides were found to fit well to a single-site binding model (eq 1), in which an individual peptide binds to the S100B dimer. The presence of only one HDM2 and HDM4 peptide binding site per S100B dimer is a distinct stoichiometry compared that of the TRTK12, p53, and NDR peptides. However, the stoichiometry of one peptide per S100B dimer has been previously observed.[49,87] Peptides derived from the tetramerization domains of p53 (distinct sequences from the peptide studied here) and p63 have been reported to bind to S100B with the same "one peptide per dimer" stoichiometry.[49,87] The binding affinity for the HDM2$^{(25-47)}$ peptide was determined here by ITC to be 0.5 ± 0.1 μM, while the affinity for the HDM4$^{(25-47)}$ peptide was almost an order of magnitude tighter (0.07 ± 0.02 μM). An order of magnitude difference in affinities between the two peptides has been previously reported.[39] Furthermore, it has been reported that the affinity for the HDM2$^{(25-47)}$ peptide is approximately an order of magnitude tighter than those of the TRTK12$^{(265-276)}$ and p53$^{(367-388)}$ peptides, in agreement with our observations (Table 1). Figure 2 shows the changes in heat capacity for both the S100B−HDM2 and S100B−HDM4 interactions, which are significantly larger than those for the other peptides examined in this study. In addition, the experimentally determined ΔC_p for the HDM4$^{(25-47)}$ peptide (−1.7 ± 0.2 kJ mol^{-1} K^{-1}) is significantly different from that obtained using homology models of the bound complex (−0.7 ± 0.1 kJ mol^{-1} K^{-1}) (see Experimental Procedures), where the stoichiometry was modeled as one peptide per S100B dimer (Table 1).

Chemical Shift Perturbations Caused by Peptide Binding. Interactions between S100B and various peptide targets were examined by monitoring binding-induced changes in the chemical shifts of backbone ^{15}N and ^{1}H atoms between the peptide-free state and the peptide-bound state (Figure 3). While resonances undergoing binding-induced chemical shift perturbations are generally limited to those atoms within the interaction surface, it should be noted that chemical shift changes can be detected in residues neighboring those that make direct contacts or in cases where structural changes involving remote sites are coupled with binding events. However, the results suggest that binding-induced chemical shift perturbations are localized to discrete interaction surfaces and that peptide binding does not induce an allosteric effect. The protein concentrations used in this study preclude a full assignment of S100B in the peptide-free and peptide-bound states. However, the majority of the amino acid residues in S100B that underwent significant chemical shift perturbations were observable and structurally cluster to a region that is in good agreement with the residues reported to be directly involved with TRTK12$^{(265-276)}$, p53$^{(367-388)}$, and NDR$^{(62-87)}$ peptide binding in previous structural studies (see Figure 3).[5,39,54] Specifically, residues from loop 2 (S41, H42, F43, L44, and E45), helix 3 (V52, V53, V56, and T59), and the C-terminus of helix 4 (S78−F88) were found to interact with the p53$^{(367-388)}$, TRTK12$^{(265-276)}$, and NDR$^{(62-87)}$ peptides. There are no structures available for S100B in complex with either HDM2$^{(25-47)}$ or HDM4$^{(25-47)}$. However, we find that the residues involved in binding the HDM2$^{(25-47)}$ and HDM4$^{(25-47)}$ peptides are very similar to those involved in binding the targets listed above, suggesting that all binding sites at least partially overlap (Figure 3). This is consistent with previous competition assays that showed that the S100B−HDM2 interaction can be disrupted by both TRTK12$^{(265-276)}$ and wild-type p53.[39] In addition, significant chemical shifts are observed for residues at the dimer interface, including S78, M79, V80, T81, T82, and A83, for the HDM2$^{(25-47)}$ and HDM4$^{(25-47)}$ peptide interactions.

Line Shape Analysis. The chemical shift changes for S100B ^{1}H and ^{15}N resonances were quantified using a series of 2D HSQC experiments with progressive increases in the peptide concentration until there were no longer observable changes in chemical shifts. These experimental data were further analyzed here to characterize the thermodynamics and kinetics of the interaction.[88,89] More specifically, line shape analysis was performed on one-dimensional line shapes extracted from the series of 2D HSQC spectra and used to obtain fits for the affinity and kinetic rate constants of binding.[88] This method is most accurate when exchange between the bound and free states is not in the extreme "fast" or "slow" exchange regimes, where K_{ex} is approximately 2 orders of magnitude greater than or lower than $\Delta\omega$, respectively. The apparent affinities and kinetic constants from the global fit analysis are listed in Tables 2−4.

TRTK12. For the TRTK12$^{(265-276)}$ titration, we established that binding occurs according to the simplest model, where

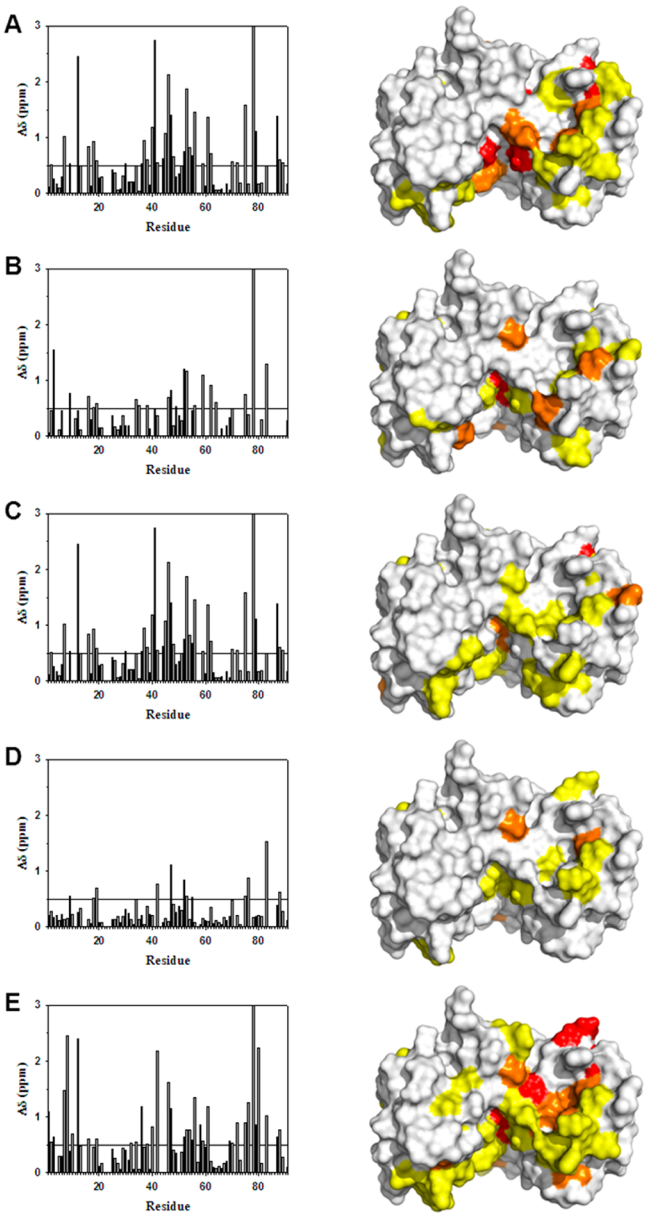

Figure 3. Changes in backbone ^{1}H and ^{15}N chemical shifts for Ca^{2+}-bound S100B upon binding various peptide targets. Similar residues in S100B undergo chemical shift perturbations upon binding $TRTK12^{(265-276)}$ (A), $p53^{(367-388)}$ (B), $NDR^{(62-87)}$ (C), $HDM2^{(25-47)}$ (D), or $HDM4^{(25-47)}$ (E). The bar graphs show the combined backbone ^{1}H and ^{15}N chemical shift perturbations upon peptide binding to Ca^{2+}-S100B. Residues without $\Delta\delta$ values underwent exchange broadening upon binding and/or could not be assigned in both the peptide-free and peptide-bound states.

there are two identical sites per S100B dimer. This is consistent with the NMR results, where a single set of chemical shifts were observed for each amino acid residue, suggesting each monomer underwent an identical binding event. In addition, few resonances were observed to have significant line broadening, allowing the population-averaged chemical shift values of the peptide-bound and peptide-free states to be tracked throughout the titration. Binding therefore occurs in the intermediate to fast exchange regime relative to the "NMR time scale" ($K_{off} \geq \Delta\omega$). The dissociation constant obtained directly from the line shape analysis is in excellent agreement with the K_d from ITC. The obtained kinetic parameters for

Table 2. Summary of the Kinetic Properties of S100B Binding to p53, TRTK12, NDR, HDM2, and HDM4 Determined Using NMR and ITC Experiments and LineShapeKin Analysis

peptide	$K_{d,app}$ (μM)[a]	K_{off} (s^{-1})	K_{on} ($\times 10^7$ M^{-1} s^{-1})
TRTK12	2 ± 0.5	110 ± 20	5 ± 2
p53, low salt	2 ± 0.5	760 ± 150	40 ± 16
p53, high salt	30 ± 6	900 ± 180	3 ± 1
NDR	0.4 ± 0.2, 2 ± 1[b]	50–250, 20–200[b]	13–63, 1–10[b]
HDM2	0.5 ± 0.2[c]	140 ± 30	30 ± 11
HDM4	0.07 ± 0.03[c]	30 ± 10	4 ± 2

[a]Peptide binding was fit to a single-site model for all peptides during the LineShapeKin analysis. All reported values are for the apparent K_d. [b]Kinetic rates could not be determined analytically. See Experimental Procedures. [c]A binding model with one peptide per S100B dimer was used. The K_d value was taken from ITC, and K_{off} was allowed to float.

Table 3. Summary of the Kinetic Properties of S100B Binding to p53, TRTK12, NDR, HDM2, and HDM4 Determined Using NMR Experiments and LineShapeKin Analysis

peptide	$K_{d,app}$ (μM)[a]	K_{off} (s^{-1})	K_{on} ($\times 10^7$ M^{-1} s^{-1})
TRTK12	1.0 ± 0.5	100 ± 20	10 ± 4
p53, low salt	1.0 ± 0.5	800 ± 160	80 ± 30
p53, high salt	10 ± 2	750 ± 150	7.5 ± 1.5
NDR	na[b]	na[b]	na[b]
HDM2	0.1 ± 0.02[c]	160 ± 30	160 ± 70
HDM4	1.0 ± 0.5[c]	30 ± 10	3 ± 1

[a]Peptide binding was fit to a single-site model for all peptides during the LineshapeKin analysis. All reported values are for the apparent K_d. [b]K_d values and kinetic rates could not be determined analytically. See Experimental Procedures and Table 1. [c]A binding model with one peptide per S100B dimer was used. K_d was taken directly from the 2D matrix. K_{off} was then allowed to float with that K_d held constant.

Table 4. Summary of the Kinetic Properties of S100B Binding to p53, TRTK12, NDR, HDM2, and HDM4 Determined Using NMR Experiments and LineShapeKin Analysis

peptide	$K_{d,app}$ (μM)[a]	K_{off} (s^{-1})	K_{on} ($\times 10^7$ M^{-1} s^{-1})
TRTK12	1.0 ± 0.5	100 ± 20	10 ± 4
p53, low salt	1.0 ± 0.5	1000 ± 200	100 ± 40
p53, high salt	10 ± 2	1000 ± 200	10 ± 2
NDR	na[b]	na[b]	na[b]
HDM2	0.1 ± 0.02[c]	100 ± 20	100 ± 40
HDM4	1.0 ± 0.5[c]	10 ± 2	1.0 ± 0.4

[a]Peptide binding was fit to a single-site model for all peptides during the LineShapeKin analysis. All reported values are for the apparent K_d. [b]K_d values and kinetic rates could not be determined analytically. See Experimental Procedures and Table 1. [c]A binding model with one peptide per S100B dimer was used. K_d and K_{off} were taken directly from the 2D matrix.

binding are as follows: $K_{on} = 1 \times 10^8 \pm 4 \times 10^7$ M^{-1} s^{-1}, and $K_{off} = 100 \pm 20$ s^{-1} (Table 3). Similar rates were obtained regardless of whether the K_d is allowed to be fit in the line shape analysis or fixed to values obtained by ITC and indicate the robustness of our analysis (Table 2). Previously, Barber et al. examined the chemical shift changes of the Trp7 indole ring

dx.doi.org/10.1021/bi300865g | Biochemistry 2012, 51, 7189–7201

of the TRTK12$^{(265-276)}$ peptide throughout a titration with S100B and estimated a K_{on} of 1.4×10^8 M^{-1} s^{-1} and a K_{off} of 125 s^{-1}.[86] These results are in excellent agreement with the kinetic rate constants observed in this study.

p53. The chemical shift changes observed for p53$^{(367-388)}$ binding to S100B are similar to those of the TRTK12$^{(265-276)}$ peptide, i.e., fast on the NMR time scale and consistent with the model with two identical binding sites per dimer, in which one peptide binds each S100B monomer. The dissociation constant calculated from line shape analysis is similar to that from ITC and results in a K_{on} of $8 \times 10^8 \pm 3.2 \times 10^7$ M^{-1} s^{-1} and a K_{off} of 800 ± 160 s^{-1} (Table 3). The K_{on} for the p53$^{(367-388)}$ peptide is the greatest of any of the peptides examined in this study. Such fast K_{on} rate constants are not frequently observed for protein−peptide interactions but have been reported. Examples include those of peptides derived from nitric oxide synthase binding to calmodulin (6.6×10^8 M^{-1} s^{-1})[90] and the phosphorylated kinase inducible domain (pKID) binding to the structured KIX domain (6.3×10^6 M^{-1} s^{-1}).[91] Interestingly, peptides derived from the N-terminus of p53$^{(17-26)}$ have been observed to bind to the MDM2 protein with a K_{on} of 2.2×10^7 M^{-1} s^{-1},[60] and p53$^{(38-61)}$ has been observed to bind to CBP with a K_{on} of 1.7×10^{10} M^{-1} s^{-1}.[92] Specifically, the binding kinetics reported for the p53 peptides in the latter study approach the theoretical limit of protein−ligand binding, even when factoring in electrostatic interactions.[93−95] Taken together, these studies indicate that fast binding kinetics may be a general property of p53−target protein interactions and that it may be important for the biological functions of p53.

NDR. A single amide peak was observed for equivalent residues of the S100B dimer with chemical shift perturbations exhibiting fast exchange behavior in binding studies with the NDR$^{(62-87)}$ peptide. While the results are consistent with earlier observations,[5,29,35] ITC analysis indicates that a sequential recognition model is employed, with two, nonidentical binding sites per S100B dimer. As a result, distinct chemical shifts for amide resonances from each monomeric unit could be anticipated because of the loss of symmetry within the dimer complex. However, the rates of exchange between free and bound states are shown here to be sufficiently rapid to result in the time-averaged chemical shifts that are being observed. Indeed, the affinities of each site differ by less than an order of magnitude according to ITC, and the exchange between the free and fully bound state is fast on the NMR time scale. Because there is no analytical solution available for the sequential binding model, one cannot explicitly calculate the kinetic rate constants using LineShapeKin.[82] Instead, the titration data were simulated[83] using the dissociation constants obtained with ITC to estimate upper and lower bounds for the kinetic parameters. The K_{off} for the first peptide binding event is estimated to be between 50 and 250 s^{-1}, while the K_{off} for the second peptide binding event is estimated to be between 10 and 200 s^{-1}. This results in a K_{on} between 1×10^8 and 6×10^8 M^{-1} s^{-1} for the first peptide binding event and a K_{on} between 1×10^7 and 1×10^8 M^{-1} s^{-1} for the second peptide binding event (Table 2). If the titration data are directly fit to the model with two identical binding sites (one peptide per S100B monomer) and the dissociation constant is restrained by the values obtained by ITC, then the K_{off} rate is estimated to be 180 ± 40 s^{-1}. This results in K_{on} values between 9×10^7 and 5×10^8 M^{-1} s^{-1}, which are in good agreement with the simulated K_{on} rate constants.

HDM2 and HDM4. Binding of the HDM2$^{(25-47)}$ and HDM4$^{(25-47)}$ peptides occurs on the intermediate and slow time scales, respectively ($K_{ex} \leq \Delta\omega$). The stoichiometry obtained for both peptides by the ITC and NMR titrations is inconsistent with a stoichiometry of two identical binding sites (one peptide per monomer) and fits best to a single-binding site model (one peptide per S100B dimer). Furthermore, the concentrations used during the shape NMR titrations were several orders of magnitude higher than the dissociation constants ($K_d < 1$ μM), where the obtained stoichiometry is the most accurate. The simplest explanation consistent with all the data is that the HDM2$^{(25-47)}$ and HDM4$^{(25-47)}$ peptides interact with S100B through a novel binding mechanism, with the interaction surface of a single peptide possibly utilizing the prototypical binding site of both monomeric units and a portion of the dimer interface. The affinities obtained by ITC and LineShapeKin for the HDM2$^{(25-47)}$ peptide are in good agreement and result in apparent K_{on} and K_{off} rates of $2.8 \times 10^8 \pm 1.1 \times 10^8$ M^{-1} s^{-1} and 140 ± 30 s^{-1}, respectively. The HDM4$^{(25-47)}$ peptide is in a slow exchange regime with S100B, making accurate fitting of the dissociation constant using line shape analysis difficult, so the K_d value (0.07 ± 0.03 μM) was taken directly from ITC. The obtained kinetic parameters ($K_{on} = 4 \times 10^7 \pm 2 \times 10^7$ M^{-1} s^{-1}, and $K_{off} = 30 \pm 10$ s^{-1}) are the slowest of any of the peptides examined here.

DISCUSSION

Thermodynamic Mechanisms of Binding. In this study, we present detailed thermodynamic analysis for five different peptides binding to calcium-saturated S100B. Even though all five peptides bind to a similar region on S100B, they interact with the protein through three unique binding mechanisms (eqs 1−3). It is well established that both the TRTK12 and p53 peptides interact with S100B according to the simplest model, where there are two identical binding sites per S100B dimer.[29,35−37,39,49,78,96] Here, we validate this model and present novel thermodynamic data for these interactions. There was significantly less information available for the S100B−NDR interaction. Our work suggests the NDR peptide interacts with S100B protein through a sequential binding model with negative cooperativity. Although a highly symmetric structure for the S100B−NDR complex has been reported, it involves the full NDR N-terminal domain in complex with bovine S100B, which differs from the sequence of human S100B at three residue positions (Val7Met, Ser62Asn, and Ile80Val).[5] Interestingly, these few changes may actually result in a significantly altered bound state for the NDR$^{(62-88)}$ peptide. Additional precedence for the differences in the conformation of the bound state is established by the available structures of TRTK12 interacting with rat and human S100B, which only differ at two positions (Glu62Asn and Ser78Ala), yet show the peptide adopting a different orientation and structure in each case.[5,35,85] When bound to human S100B, it remains in an extended conformation, forming multiple contacts with helix 3, the loop region, and helix 4 of the protein. When bound to rat S100B, it forms a short helix, and the N-terminal region of the peptide is aligned more closely with helix 4 of S100B. The interactions between S100B and the HDM2$^{(25-47)}$ and HDM4$^{(25-47)}$ peptides are even less well understood than those of the other targets examined in this study, with no structural information available. This study suggests both the HDM2$^{(25-47)}$ and HDM4$^{(25-47)}$ peptides interact with the S100B protein with a stoichiometry of one peptide per S100B

dimer. Considering that a single protein is able to bind multiple targets with unique mechanisms, this suggests a certain degree of promiscuity in the S100B binding site, similar to that of calmodulin.[97] It appears that this is a general property of the S100 proteins. For example, the interactions between the Annexin I peptide and S100A11 are best described by a model with two identical binding sites, while the interactions of the Annexin II peptide with the same protein are best described by a model with two sequential binding sites.[65]

The promiscuity of the S100 binding site is also evident at the structural level. The difference in the orientation of the TRTK12 peptide in complex with human and bovine S100B proteins has been discussed above. The binding of the non-muscle myosin IIA peptide fragment to S100A4[98] is another stark example. It shows a stoichiometry of one peptide per S100A4 dimer, with the peptide occupying binding sites on both monomers. In general, the peptide binding site on the S100 proteins is defined by residues from helix 3, the loop region, and helix 4, but the orientation of different peptides bound to this site is very distinct (Figure 4).

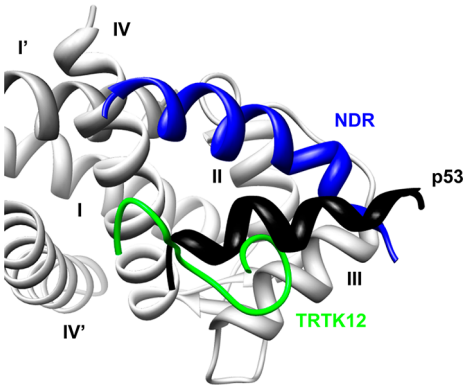

Figure 4. S100 proteins interact with peptide targets through a promiscuous binding site. Ribbon cartoon representing the converged NMR ensemble for the S100B protein interacting with the TRTK12 (green, PDB entry 1MQ1), p53 (black, PDB entry 1DT7), and NDR (blue, PDB entry 1PBS) peptides in the presence of calcium. Only the binding site of one S100B monomer (light gray, helices I–IV) is shown. Although all three peptides interact with similar amino acid residues in the binding pocket of S100B with the same stoichiometry, each peptide binds in a unique orientation with a distinct structure.

This difference in peptide orientation in the binding site and dissociation constants partially originates from the variations in peptide sequences. It has been proposed that the S100B binding motif consists of a core of hydrophobic residues flanked by positively charged Arg or Lys residues on one side or both sides.[39] The importance of hydrophobic residues for binding is evident in the large negative heat capacity change upon binding for all peptides studied both here (Table 1) and in previous work.[65,69,70,73] Of these, the HDM2$^{(25-47)}$ and HDM4$^{(25-47)}$ peptides have the largest absolute values of ΔC_p and also have the tightest binding affinities for S100B (Table 1). Importantly, both peptides contain the largest fraction of nonpolar residues in their sequences. This suggests that the percent hydrophobicity of a peptide is an important parameter when defining the binding affinity for S100B. The aliphatic index for HDM2$^{(25-47)}$ and HDM4$^{(25-47)}$ is several times higher than those of similarly sized ligands, including the NDR$^{(62-87)}$, p53$^{(367-388)}$, and RAGE$^{(42-59)}$ peptides.[99] Interestingly, one of the only other peptides known to bind S100B with submicromolar affinity, ROS-GC1$^{(962-981)}$, shares these same features. The majority of the residues in this peptide are also nonpolar, and the aliphatic index is similar to that of the HDM peptides, thus supporting the importance of hydrophobicity for the dissociation constant for S100B.

Kinetic Mechanism of Binding. Interactions between S100B and its peptide targets reveal complex and coupled folding and binding events. Previous studies have observed that binding of p53 induces helical formation in the peptide.[38] In contrast, TRTK12$^{(265-276)}$ in complex with rat S100B was observed to have a single helical turn but to remain completely unstructured in complex with human S100B.[5,54] For NDR$^{(62-87)}$, more than half of the peptide adopts a helical structure in the bound state.[5] There are no available structures for the S100B–HDM2 or S100B–HDM4 complex.

This study is the first to experimentally examine the kinetics of peptide binding to S100B and its implication for the coupled binding and folding mechanism. While the exact time constants of helix formation are still in dispute, it is generally accepted that the coil–helix transition takes place in less than 1 μs, with residues first slowly overcoming the high energy barrier for nucleation and then becoming elongated with a time constant proportional to the number of residues in the final helix.[100,101] All five peptides were predicted to be unstructured in the unbound state using the Agadir algorithm, and the lack of significant secondary structure content was subsequently confirmed by CD spectroscopy (see the Supporting Information). This strongly suggests these peptides can be considered to be intrinsically disordered (IDP's),[92] i.e., that the folded state for the peptide found in the final complex with S100B exists only transiently in the unbound state. We find a fly casting or folding after binding mechanism[102,103] to be the most likely explanation for the large observed bimolecular rates for these peptides, as opposed to conformational selection.[104,105] The distinction between these two mechanisms for peptides that become structured in the bound state can be made from the analysis of the K_{on} rates.[106] It is generally considered that the fly casting mechanism for such systems has a K_{on} on the order of 10^7–10^{10} M^{-1} s^{-1}, while the conformational selection mechanism has been proposed to have a K_{on} slower than 10^7 M^{-1} s^{-1}.[106] For the p53$^{(367-388)}$ and NDR$^{(62-87)}$ peptides, electrostatic steering between the positively charged Arg and Lys residues of the ligands and the negatively charged Glu residues in the S100B binding pocket may also contribute significantly to the large K_{on} values. This is directly supported by experimental evidence. For the interaction of p53$^{(367-388)}$ with S100B, K_{on} is reduced by an order of magnitude in the presence of 120 mM NaCl, resulting in a similar reduction in the dissociation constant (Tables 1 and 2). Several computational simulations that have examined the S100B–p53 interaction specifically,[52,107] and the binding of unstructured ligands in general,[52,102,106,108–111] have arrived at a similar conclusion, namely, that folding after binding is the principal mechanism for these species. Unfortunately, only a limited number of experimental studies have examined this hypothesis.[91,92,112–114] The kinetic results reported here represent an important contribution to the growing body of evidence for this fly casting mechanism.

■ ASSOCIATED CONTENT

Supporting Information

Supplementary methods and Figures S1–S3. This material is available free of charge via the Internet at http://pubs.acs.org.

dx.doi.org/10.1021/bi300865g | *Biochemistry* 2012, 51, 7189–7201

AUTHOR INFORMATION

Corresponding Author

*Phone: (518) 276-4417. Fax: (518) 276-2851. E-mail: makhag@rpi.edu.

Present Address

[†]NNF Center for Protein Research, University of Copenhagen, Blegdamsvej 3B, DK-2200 Copenhagen N, Denmark.

Funding

This work was supported by National Institute of General Medical Sciences Grant RO1-GM054537.

Notes

The authors declare no competing financial interest.

ACKNOWLEDGMENTS

Instrumentation at the Core Facilities at the Center of Biotechnology and Interdisciplinary Studies was used for some of the experiments reported in this paper. We thank Anthony Chiarella for his contributions to protein expression and purification and Dr. Evgenii Kovrigin for providing advice about the usage of LineShapeKin.

ABBREVIATIONS

CD, circular dichroism; EDTA, ethylenediaminetetraacetic acid; EF-hand, calcium-binding domain consisting of a helix−loop−helix structure; Fmoc, fluorenylmethyloxycarbonyl chloride; HDM2, human homologue of murine double minute 2 protein; HDM4, human homologue of murine double minute 4 protein; HSQC, heteronuclear single-quantum coherence; IPTG, isopropyl β-D-thiogalactopyranoside; ITC, isothermal titration calorimetry; MDM2, murine double minute 2; MDM4, murine double minute 4; NDR, nuclear Dbf2-related kinase; NMR, nuclear magnetic resonance; TCEP, tris(2-carboxyethyl)phosphine; TFE, trifluoroethanol; UV, ultraviolet.

REFERENCES

(1) Schafer, B. W., and Heizmann, C. W. (1996) The S100 family of EF-hand calcium-binding proteins: Functions and pathology. *Trends Biochem. Sci. 21*, 134−140.

(2) Pritchard, K., and Marston, S. B. (1991) Ca^{2+}-dependent regulation of vascular smooth-muscle caldesmon by S.100 and related smooth-muscle proteins. *Biochem. J. 277* (Part 3), 819−824.

(3) Wilder, P. T., Rustandi, R. R., Drohat, A. C., and Weber, D. J. (1998) S100B(ββ) inhibits the protein kinase C-dependent phosphorylation of a peptide derived from p53 in a Ca^{2+}-dependent manner. *Protein Sci. 7*, 794−798.

(4) Heierhorst, J., Kobe, B., Feil, S. C., Parker, M. W., Benian, G. M., Weiss, K. R., and Kemp, B. E. (1996) Ca^{2+}/S100 regulation of giant protein kinases. *Nature 380*, 636−639.

(5) Bhattacharya, S., Large, E., Heizmann, C. W., Hemmings, B., and Chazin, W. J. (2003) Structure of the Ca^{2+}/S100B/NDR kinase peptide complex: Insights into S100 target specificity and activation of the kinase. *Biochemistry 42*, 14416−14426.

(6) Sorci, G., Agneletti, A. L., and Donato, R. (2000) Effects of S100A1 and S100B on microtubule stability. An in vitro study using triton-cytoskeletons from astrocyte and myoblast cell lines. *Neuroscience 99*, 773−783.

(7) Tarabykina, S., Scott, D. J., Herzyk, P., Hill, T. J., Tame, J. R., Kriajevska, M., Lafitte, D., Derrick, P. J., Dodson, G. G., Maitland, N. J., Lukanidin, E. M., and Bronstein, I. B. (2001) The dimerization interface of the metastasis-associated protein S100A4 (Mts1): In vivo and in vitro studies. *J. Biol. Chem. 276*, 24212−24222.

(8) Gibadulinova, A., Tothova, V., Pastorek, J., and Pastorekova, S. (2011) Transcriptional regulation and functional implication of S100P in cancer. *Amino Acids 41*, 885−892.

(9) Nakazato, Y., Ishizeki, J., Takahashi, K., and Yamaguchi, H. (1982) Immunohistochemical localization of S-100 protein in granular cell myoblastoma. *Cancer 49*, 1624−1628.

(10) Salama, I., Malone, P. S., Mihaimeed, F., and Jones, J. L. (2008) A review of the S100 proteins in cancer. *European Journal of Surgical Oncology. 34*, 357−364.

(11) Goyette, J., and Geczy, C. L. (2010) Inflammation-associated S100 proteins: New mechanisms that regulate function. *Amino Acids 41*, 821−842.

(12) Leclerc, E., Fritz, G., Vetter, S. W., and Heizmann, C. W. (2009) Binding of S100 proteins to RAGE: An update. *Biochim. Biophys. Acta 1793*, 993−1007.

(13) Moroz, O. V., Burkitt, W., Wittkowski, H., He, W., Ianoul, A., Novitskaya, V., Xie, J., Polyakova, O., Lednev, I. K., Shekhtman, A., Derrick, P. J., Bjoerk, P., Foell, D., and Bronstein, I. B. (2009) Both Ca^{2+} and Zn^{2+} are essential for S100A12 protein oligomerization and function. *BMC Biochem. 10*, 11.

(14) Liu, J., Wang, H., Zhang, L., Xu, Y., Deng, W., Zhu, H., and Qin, C. (2011) S100B transgenic mice develop features of Parkinson's disease. *Arch. Med. Res. 42*, 1−7.

(15) Esposito, G., Imitola, J., Lu, J., De Filippis, D., Scuderi, C., Ganesh, V. S., Folkerth, R., Hecht, J., Shin, S., Iuvone, T., Chesnut, J., Steardo, L., and Sheen, V. (2008) Genomic and functional profiling of human Down syndrome neural progenitors implicates S100B and aquaporin 4 in cell injury. *Hum. Mol. Genet. 17*, 440−457.

(16) Chaves, M. L., Camozzato, A. L., Ferreira, E. D., Piazenski, I., Kochhann, R., Dall'igna, O., Mazzini, G. S., Souza, D. O., and Portela, L. V. (2010) Serum levels of S100B and NSE proteins in Alzheimer's disease patients. *J. Neuroinflammation 7*, 6.

(17) Leclerc, E., Sturchler, E., and Vetter, S. W. (2010) The S100B/RAGE Axis in Alzheimer's Disease. *Cardiovasc. Psychiatry Neurol. 2010*, 539581.

(18) Donato, R. (2003) Intracellular and extracellular roles of S100 proteins. *Microsc. Res. Tech. 60*, 540−551.

(19) Fritz, G., and Heizmann, C. W. (2011) 3D Structures of the Calcium and Zinc Binding S100 Proteins. In *Encyclopedia of Inorganic and Bioinorganic Chemistry*, John Wiley & Sons, Ltd., New York.

(20) Henzl, M. T., Davis, M. E., and Tan, A. (2008) Leucine 85 is an important determinant of divalent ion affinity in rat β-parvalbumin (oncomodulin). *Biochemistry 47*, 13635−13646.

(21) Henzl, M. T., and Tanner, J. J. (2007) Solution structure of Ca^{2+}-free rat β-parvalbumin (oncomodulin). *Protein Sci. 16*, 1914−1926.

(22) Isobe, T., and Okuyama, T. (1978) The amino-acid sequence of S-100 protein (PAP I-b protein) and its relation to the calcium-binding proteins. *Eur. J. Biochem. 89*, 379−388.

(23) Potts, B. C., Smith, J., Akke, M., Macke, T. J., Okazaki, K., Hidaka, H., Case, D. A., and Chazin, W. J. (1995) The structure of calcyclin reveals a novel homodimeric fold for S100 Ca^{2+}-binding proteins. *Nat. Struct. Biol. 2*, 790−796.

(24) Drohat, A. C., Baldisseri, D. M., Rustandi, R. R., and Weber, D. J. (1998) Solution structure of calcium-bound rat S100B(ββ) as determined by nuclear magnetic resonance spectroscopy. *Biochemistry 37*, 2729−2740.

(25) Kilby, P. M., Van Eldik, L. J., and Roberts, G. C. (1996) The solution structure of the bovine S100B protein dimer in the calcium-free state. *Structure 4*, 1041−1052.

(26) Matsumura, H., Shiba, T., Inoue, T., Harada, S., and Kai, Y. (1998) A novel mode of target recognition suggested by the 2.0 Å structure of holo S100B from bovine brain. *Structure 6*, 233−241.

(27) Smith, S. P., and Shaw, G. S. (1998) A novel calcium-sensitive switch revealed by the structure of human S100B in the calcium-bound form. *Structure 6*, 211−222.

(28) Maler, L., Potts, B. C., and Chazin, W. J. (1999) High resolution solution structure of apo calcyclin and structural variations in the S100 family of calcium-binding proteins. *J. Biomol. NMR 13*, 233−247.

(29) Rustandi, R. R., Baldisseri, D. M., and Weber, D. J. (2000) Structure of the negative regulatory domain of p53 bound to S100B(ββ). *Nat. Struct. Biol. 7*, 570−574.

(30) Santamaria-Kisiel, L., Rintala-Dempsey, A. C., and Shaw, G. S. (2006) Calcium-dependent and -independent interactions of the S100 protein family. *Biochem. J. 396*, 201−214.
(31) Moore, B. (1965) A soluble protein characteristic of the nervous system. *Biochem. Biophys. Res. Commun. 19*, 739−744.
(32) Bernstein, F. C., Koetzle, T. F., Williams, G. J., Meyer, E. F., Jr., Brice, M. D., Rodgers, J. R., Kennard, O., Shimanouchi, T., and Tasumi, M. (1977) The Protein Data Bank. A computer-based archival file for macromolecular structures. *Eur. J. Biochem. 80*, 319−324.
(33) Nonaka, D., Chiriboga, L., and Rubin, B. P. (2008) Differential expression of S100 protein subtypes in malignant melanoma, and benign and malignant peripheral nerve sheath tumors. *J. Cutaneous Pathol. 35*, 1014−1019.
(34) Rezvanpour, A., Phillips, J. M., and Shaw, G. S. (2009) Design of high-affinity S100-target hybrid proteins. *Protein Sci. 18*, 2528−2536.
(35) Inman, K. G., Yang, R., Rustandi, R. R., Miller, K. E., Baldisseri, D. M., and Weber, D. J. (2002) Solution NMR structure of S100B bound to the high-affinity target peptide TRTK-12. *J. Mol. Biol. 324*, 1003−1014.
(36) Rustandi, R. R., Drohat, A. C., Baldisseri, D. M., Wilder, P. T., and Weber, D. J. (1998) The Ca^{2+}-dependent interaction of S100B($\beta\beta$) with a peptide derived from p53. *Biochemistry 37*, 1951−1960.
(37) Fernandez-Fernandez, M. R., Rutherford, T. J., and Fersht, A. R. (2008) Members of the S100 family bind p53 in two distinct ways. *Protein Sci. 17*, 1663−1670.
(38) Rustandi, R. R., Baldisseri, D. M., Drohat, A. C., and Weber, D. J. (1999) Structural changes in the C-terminus of Ca^{2+}-bound rat S100B($\beta\beta$) upon binding to a peptide derived from the C-terminal regulatory domain of p53. *Protein Sci. 8*, 1743−1751.
(39) Wilder, P. T., Lin, J., Bair, C. L., Charpentier, T. H., Yang, D., Liriano, M., Varney, K. M., Lee, A., Oppenheim, A. B., Adhya, S., Carrier, F., and Weber, D. J. (2006) Recognition of the tumor suppressor protein p53 and other protein targets by the calcium-binding protein S100B. *Biochim. Biophys. Acta 1763*, 1284−1297.
(40) van Dieck, J., Lum, J. K., Teufel, D. P., and Fersht, A. R. (2010) S100 proteins interact with the N-terminal domain of MDM2. *FEBS Lett. 584*, 3269−3274.
(41) Rety, S., Sopkova, J., Renouard, M., Osterloh, D., Gerke, V., Tabaries, S., Russo-Marie, F., and Lewit-Bentley, A. (1999) The crystal structure of a complex of p11 with the annexin II N-terminal peptide. *Nat. Struct. Biol. 6*, 89−95.
(42) Rety, S., Osterloh, D., Arie, J. P., Tabaries, S., Seeman, J., Russo-Marie, F., Gerke, V., and Lewit-Bentley, A. (2000) Structural basis of the Ca^{2+}-dependent association between S100C (S100A11) and its target, the N-terminal part of annexin I. *Structure 8*, 175−184.
(43) Gribenko, A. V., and Makhatadze, G. I. (1998) Oligomerization and divalent ion binding properties of the S100P protein: A Ca^{2+}/Mg^{2+}-switch model. *J. Mol. Biol. 283*, 679−694.
(44) Pozdnyakov, N., Margulis, A., and Sitaramayya, A. (1998) Identification of effector binding sites on S100β: Studies with guanylate cyclase and p80, a retinal phosphoprotein. *Biochemistry 37*, 10701−10708.
(45) Garbuglia, M., Verzini, M., Rustandi, R. R., Osterloh, D., Weber, D. J., Gerke, V., and Donato, R. (1999) Role of the C-terminal extension in the interaction of S100A1 with GFAP, tubulin, the S100A1- and S100B-inhibitory peptide, TRTK-12, and a peptide derived from p53, and the S100A1 inhibitory effect on GFAP polymerization. *Biochem. Biophys. Res. Commun. 254*, 36−41.
(46) Ivanenkov, V. V., Jamieson, G. A., Jr., Gruenstein, E., and Dimlich, R. V. (1995) Characterization of S-100b binding epitopes. Identification of a novel target, the actin capping protein, CapZ. *J. Biol. Chem. 270*, 14651−14658.
(47) Ashcroft, M., Kubbutat, M. H., and Vousden, K. H. (1999) Regulation of p53 function and stability by phosphorylation. *Mol. Cell. Biol. 19*, 1751−1758.
(48) Tyner, S. D., Venkatachalam, S., Choi, J., Jones, S., Ghebranious, N., Igelmann, H., Lu, X., Soron, G., Cooper, B., Brayton, C., Hee Park, S., Thompson, T., Karsenty, G., Bradley, A., and Donehower, L. A. (2002) p53 mutant mice that display early ageing-associated phenotypes. *Nature 415*, 45−53.
(49) Fernandez-Fernandez, M. R., Veprintsev, D. B., and Fersht, A. R. (2005) Proteins of the S100 family regulate the oligomerization of p53 tumor suppressor. *Proc. Natl. Acad. Sci. U.S.A. 102*, 4735−4740.
(50) van Dieck, J., Fernandez-Fernandez, M. R., Veprintsev, D. B., and Fersht, A. R. (2009) Modulation of the oligomerization state of p53 by differential binding of proteins of the S100 family to p53 monomers and tetramers. *J. Biol. Chem. 284*, 13804−13811.
(51) Bell, S., Klein, C., Muller, L., Hansen, S., and Buchner, J. (2002) p53 contains large unstructured regions in its native state. *J. Mol. Biol. 322*, 917−927.
(52) Chen, J. (2009) Intrinsically disordered p53 extreme C-terminus binds to S100B($\beta\beta$) through "fly-casting". *J. Am. Chem. Soc. 131*, 2088−2089.
(53) Oldfield, C. J., Meng, J., Yang, J. Y., Yang, M. Q., Uversky, V. N., and Dunker, A. K. (2008) Flexible nets: Disorder and induced fit in the associations of p53 and 14-3-3 with their partners. *BMC Genomics 9* (Suppl. 1), S1.
(54) Charpentier, T. H., Thompson, L. E., Liriano, M. A., Varney, K. M., Wilder, P. T., Pozharski, E., Toth, E. A., and Weber, D. J. (2010) The effects of CapZ peptide (TRTK-12) binding to S100B-Ca^{2+} as examined by NMR and X-ray crystallography. *J. Mol. Biol. 396*, 1227−1243.
(55) Liriano, M., Varney, K., Wright, N., Hoffman, C., Toth, E., Ishima, R., and Weber, D. (2012) Target Binding to S100B Reduces Dynamic Properties and Increases Ca^{2+}-Binding Affinity for Wild Type and EF-Hand Mutant Proteins. *J. Mol. Biol.*, PMID: 22824086.
(56) Markowitz, J., Rustandi, R. R., Varney, K. M., Wilder, P. T., Udan, R., Wu, S. L., Horrocks, W. D., and Weber, D. J. (2005) Calcium-binding properties of wild-type and EF-hand mutants of S100B in the presence and absence of a peptide derived from the C-terminal negative regulatory domain of p53. *Biochemistry 44*, 7305−7314.
(57) Hergovich, A., Stegert, M. R., Schmitz, D., and Hemmings, B. A. (2006) NDR kinases regulate essential cell processes from yeast to humans. *Nat. Rev. Mol. Cell Biol. 7*, 253−264.
(58) Tamaskovic, R., Bichsel, S. J., Rogniaux, H., Stegert, M. R., and Hemmings, B. A. (2003) Mechanism of Ca^{2+}-mediated regulation of NDR protein kinase through autophosphorylation and phosphorylation by an upstream kinase. *J. Biol. Chem. 278*, 6710−6718.
(59) Francoz, S., Froment, P., Bogaerts, S., De Clercq, S., Maetens, M., Doumont, G., Bellefroid, E., and Marine, J. C. (2006) Mdm4 and Mdm2 cooperate to inhibit p53 activity in proliferating and quiescent cells in vivo. *Proc. Natl. Acad. Sci. U.S.A. 103*, 3232−3237.
(60) Schon, O., Friedler, A., Bycroft, M., Freund, S. M., and Fersht, A. R. (2002) Molecular mechanism of the interaction between MDM2 and p53. *J. Mol. Biol. 323*, 491−501.
(61) Mancini, F., Di Conza, G., Monti, O., Macchiarulo, A., Pellicciari, R., Pontecorvi, A., and Moretti, F. (2010) Puzzling over MDM4-p53 network. *Int. J. Biochem. Cell Biol. 42*, 1080−1083.
(62) Linke, K., Mace, P. D., Smith, C. A., Vaux, D. L., Silke, J., and Day, C. L. (2008) Structure of the MDM2/MDMX RING domain heterodimer reveals dimerization is required for their ubiquitylation in trans. *Cell Death Differ. 15*, 841−848.
(63) Sanchez, M. C., Renshaw, J. G., Davies, G., Barlow, P. N., and Vogtherr, M. (2010) MDM4 binds ligands via a mechanism in which disordered regions become structured. *FEBS Lett. 584*, 3035−3041.
(64) Gribenko, A., Lopez, M. M., Richardson, J. M., III, and Makhatadze, G. I. (1998) Cloning, overexpression, purification, and spectroscopic characterization of human S100P. *Protein Sci. 7*, 211−215.
(65) Streicher, W. W., Lopez, M. M., and Makhatadze, G. I. (2009) Annexin I and annexin II N-terminal peptides binding to S100 protein family members: Specificity and thermodynamic characterization. *Biochemistry 48*, 2788−2798.
(66) Gribenko, A. V., Hopper, J. E., and Makhatadze, G. I. (2001) Molecular characterization and tissue distribution of a novel member

of the S100 family of EF-hand proteins. *Biochemistry 40*, 15538−15548.
(67) Wright, N. T., Cannon, B. R., Wilder, P. T., Morgan, M. T., Varney, K. M., Zimmer, D. B., and Weber, D. J. (2009) Solution structure of S100A1 bound to the CapZ peptide (TRTK12). *J. Mol. Biol. 386*, 1265−1277.
(68) Wilkins, M. R., Gasteiger, E., Bairoch, A., Sanchez, J. C., Williams, K. L., Appel, R. D., and Hochstrasser, D. F. (1999) Protein identification and analysis tools in the ExPASy server. *Methods Mol. Biol. 112*, 531−552.
(69) Gribenko, A. V., Guzman-Casado, M., Lopez, M. M., and Makhatadze, G. I. (2002) Conformational and thermodynamic properties of peptide binding to the human S100P protein. *Protein Sci. 11*, 1367−1375.
(70) Lopez, M. M., and Makhatadze, G. I. (2002) Isothermal titration calorimetry. *Methods Mol. Biol. 173*, 121−126.
(71) Wiseman, T., Williston, S., Brandts, J. F., and Lin, L. N. (1989) Rapid measurement of binding constants and heats of binding using a new titration calorimeter. *Anal. Biochem. 179*, 131−137.
(72) Rohl, C. A., and Baldwin, R. L. (1998) Deciphering rules of helix stability in peptides. *Methods Enzymol. 295*, 1−26.
(73) Brokx, R. D., Lopez, M. M., Vogel, H. J., and Makhatadze, G. I. (2001) Energetics of target peptide binding by calmodulin reveals different modes of binding. *J. Biol. Chem. 276*, 14083−14091.
(74) Makhatadze, G. I., and Privalov, P. L. (1995) Energetics of protein structure. *Adv. Protein Chem. 47*, 307−425.
(75) Eswar, N., Webb, B., Marti-Renom, M. A., Madhusudhan, M. S., Eramian, D., Shen, M. Y., Pieper, U., and Sali, A. (2007) Comparative protein structure modeling using MODELLER. *Current Protocols in Protein Science*, Chapter 2, Unit 2, p 9, Wiley, New York.
(76) Wafer, L. N., Streicher, W. W., and Makhatadze, G. I. (2010) Thermodynamics of the Trp-cage miniprotein unfolding in urea. *Proteins 78*, 1376−1381.
(77) Hitchens, T. K., Lukin, J. A., Zhan, Y., McCallum, S. A., and Rule, G. S. (2003) MONTE: An automated Monte Carlo based approach to nuclear magnetic resonance assignment of proteins. *J. Biomol. NMR 25*, 1−9.
(78) McClintock, K. A., and Shaw, G. S. (2002) Letter to the Editor: Assignments of ^{1}H, ^{13}C and ^{15}N resonances of human Ca^{2+}-S100B in complex with the TRTK-12 peptide. *J. Biomol. NMR 23*, 255−256.
(79) Rule, G. S., and Hitchens, T. K. (2005) *Fundamentals of Protein NMR Spectroscopy*, Springer, New York.
(80) Farmer, B. T., II, Constantine, K. L., Goldfarb, V., Friedrichs, M. S., Wittekind, M., Yanchunas, J., Jr., Robertson, J. G., and Mueller, L. (1996) Localizing the $NADP^{+}$ binding site on the MurB enzyme by NMR. *Nat. Struct. Biol. 3*, 995−997.
(81) Goddard, K. (2008) *Sparky* (http://www.cgl.ucsf.edu/home/sparky/).
(82) Kovrigin, E. L., and Loria, J. P. (2006) Enzyme dynamics along the reaction coordinate: Critical role of a conserved residue. *Biochemistry 45*, 2636−2647.
(83) Kovriguine, E. (2009) *LineShapeKin Simulation*, version 4.1 (http://www.lineshapekin.net).
(84) Garcia-Fuentes, L., Baron, C., and Mayorga, O. L. (1998) Influence of dynamic power compensation in an isothermal titration microcalorimeter. *Anal. Chem. 70*, 4615−4623.
(85) McClintock, K. A., and Shaw, G. S. (2003) A novel S100 target conformation is revealed by the solution structure of the Ca^{2+}-S100B-TRTK-12 complex. *J. Biol. Chem. 278*, 6251−6257.
(86) Barber, K. R., McClintock, K. A., Jamieson, G. A., Jr., Dimlich, R. V., and Shaw, G. S. (1999) Specificity and Zn^{2+} enhancement of the S100B binding epitope TRTK-12. *J. Biol. Chem. 274*, 1502−1508.
(87) van Dieck, J., Brandt, T., Teufel, D. P., Veprintsev, D. B., Joerger, A. C., and Fersht, A. R. (2010) Molecular basis of S100 proteins interacting with the p53 homologs p63 and p73. *Oncogene 29*, 2024−2035.
(88) McCallum, S. A., Hitchens, T. K., Torborg, C., and Rule, G. S. (2000) Ligand-induced changes in the structure and dynamics of a human class Mu glutathione S-transferase. *Biochemistry 39*, 7343−7356.
(89) Lian, L.-Y., and Roberts, G. C. K. (1993) *NMR of Macromolecules*, IRL Press, Oxford, U.K.
(90) Wu, G., Berka, V., and Tsai, A. L. (2011) Binding kinetics of calmodulin with target peptides of three nitric oxide synthase isozymes. *J. Inorg. Biochem. 105*, 1226−1237.
(91) Sugase, K., Dyson, H. J., and Wright, P. E. (2007) Mechanism of coupled folding and binding of an intrinsically disordered protein. *Nature 447*, 1021−1025.
(92) Arai, M., Ferreon, J. C., and Wright, P. E. (2012) Quantitative Analysis of Multisite Protein-Ligand Interactions by NMR: Binding of Intrinsically Disordered p53 Transactivation Subdomains with the TAZ2 Domain of CBP. *J. Am. Chem. Soc. 134*, 3792−3803.
(93) Berg, O. G., and von Hippel, P. H. (1985) Diffusion-controlled macromolecular interactions. *Annu. Rev. Biophys. Biophys. Chem. 14*, 131−160.
(94) Zhou, G., Wong, M. T., and Zhou, G. Q. (1983) Diffusion-controlled reactions of enzymes. An approximate analytic solution of Chou's model. *Biophys. Chem. 18*, 125−132.
(95) Zhou, G. Q., and Zhong, W. Z. (1982) Diffusion-controlled reactions of enzymes. A comparison between Chou's model and Alberty-Hammes-Eigen's model. *Eur. J. Biochem. 128*, 383−387.
(96) Wright, N. T., Varney, K. M., Ellis, K. C., Markowitz, J., Gitti, R. K., Zimmer, D. B., and Weber, D. J. (2005) The three-dimensional solution structure of Ca^{2+}-bound S100A1 as determined by NMR spectroscopy. *J. Mol. Biol. 353*, 410−426.
(97) Yamniuk, A. P., and Vogel, H. J. (2004) Calmodulin's flexibility allows for promiscuity in its interactions with target proteins and peptides. *Mol. Biotechnol. 27*, 33−57.
(98) Kiss, B., Duelli, A., Radnai, L., Kekesi, K. A., Katona, G., and Nyitray, L. (2012) Crystal structure of the S100A4-nonmuscle myosin IIA tail fragment complex reveals an asymmetric target binding mechanism. *Proc. Natl. Acad. Sci. U.S.A. 109*, 6048−6053.
(99) Ikai, A. (1980) Thermostability and aliphatic index of globular proteins. *J. Biochem. 88*, 1895−1898.
(100) De Sancho, D., and Best, R. B. (2011) What is the time scale for α-helix nucleation? *J. Am. Chem. Soc. 133*, 6809−6816.
(101) Serrano, A. L., Tucker, M. J., and Gai, F. (2011) Direct assessment of the α-helix nucleation time. *J. Phys. Chem. B 115*, 7472−7478.
(102) Shoemaker, B. A., Portman, J. J., and Wolynes, P. G. (2000) Speeding molecular recognition by using the folding funnel: The fly-casting mechanism. *Proc. Natl. Acad. Sci. U.S.A. 97*, 8868−8873.
(103) Koshland, D. E. (1958) Application of a Theory of Enzyme Specificity to Protein Synthesis. *Proc. Natl. Acad. Sci. U.S.A. 44*, 98−104.
(104) Berger, C., Weber-Bornhauser, S., Eggenberger, J., Hanes, J., Pluckthun, A., and Bosshard, H. R. (1999) Antigen recognition by conformational selection. *FEBS Lett. 450*, 149−153.
(105) Foote, J., and Milstein, C. (1994) Conformational isomerism and the diversity of antibodies. *Proc. Natl. Acad. Sci. U.S.A. 91*, 10370−10374.
(106) Kiefhaber, T., Bachmann, A., and Jensen, K. S. (2011) Dynamics and mechanisms of coupled protein folding and binding reactions. *Curr. Opin. Struct. Biol. 22*, 21−29.
(107) Ganguly, D., and Chen, J. (2011) Topology-based modeling of intrinsically disordered proteins: Balancing intrinsic folding and intermolecular interactions. *Proteins 79*, 1251−1266.
(108) Trizac, E., Levy, Y., and Wolynes, P. G. (2010) Capillarity theory for the fly-casting mechanism. *Proc. Natl. Acad. Sci. U.S.A. 107*, 2746−2750.
(109) Huang, Y., and Liu, Z. (2009) Kinetic advantage of intrinsically disordered proteins in coupled folding-binding process: A critical assessment of the "fly-casting" mechanism. *J. Mol. Biol. 393*, 1143−1159.
(110) Turjanski, A. G., Gutkind, J. S., Best, R. B., and Hummer, G. (2008) Binding-induced folding of a natively unstructured transcription factor. *PLoS Comput. Biol. 4*, e1000060.

(111) Verkhivker, G. M., Bouzida, D., Gehlhaar, D. K., Rejto, P. A., Freer, S. T., and Rose, P. W. (2003) Simulating disorder-order transitions in molecular recognition of unstructured proteins: Where folding meets binding. *Proc. Natl. Acad. Sci. U.S.A. 100*, 5148−5153.
(112) Narayanan, R., Ganesh, O. K., Edison, A. S., and Hagen, S. J. (2008) Kinetics of folding and binding of an intrinsically disordered protein: The inhibitor of yeast aspartic proteinase YPrA. *J. Am. Chem. Soc. 130*, 11477−11485.
(113) Onitsuka, M., Kamikubo, H., Yamazaki, Y., and Kataoka, M. (2008) Mechanism of induced folding: Both folding before binding and binding before folding can be realized in staphylococcal nuclease mutants. *Proteins 72*, 837−847.
(114) Bachmann, A., Wildemann, D., Praetorius, F., Fischer, G., and Kiefhaber, T. (2011) Mapping backbone and side-chain interactions in the transition state of a coupled protein folding and binding reaction. *Proc. Natl. Acad. Sci. U.S.A. 108*, 3952−3957.